# Two-Dimensional Transition Metal Dichalcogenides under Electron Irradiation: Defect Production and Doping

Hannu-Pekka Komsa,[1] Jani Kotakoski,[1,2] Simon Kurasch,[3] Ossi Lehtinen,[1]
Ute Kaiser,[3] and Arkady V. Krasheninnikov[1,4]

[1]*Department of Physics, University of Helsinki, P.O. Box 43, 00014 Helsinki, Finland*
[2]*Department of Physics, University of Vienna, Boltzmanngasse 5, 1190 Wien, Austria*
[3]*Central Facility for Electron Microscopy, Group of Electron Microscopy of Materials Science,*
*University of Ulm, 89081 Ulm, Germany*
[4]*Department of Applied Physics, Aalto University, P.O. Box 11100, 00076 Aalto, Finland*

Using first-principles atomistic simulations, we study the response of atomically thin layers of transition metal dichalcogenides (TMDs)—a new class of two-dimensional inorganic materials with unique electronic properties—to electron irradiation. We calculate displacement threshold energies for atoms in 21 different compounds and estimate the corresponding electron energies required to produce defects. For a representative structure of $MoS_2$, we carry out high-resolution transmission electron microscopy experiments and validate our theoretical predictions via observations of vacancy formation under exposure to an 80 keV electron beam. We further show that TMDs can be doped by filling the vacancies created by the electron beam with impurity atoms. Thereby, our results not only shed light on the radiation response of a system with reduced dimensionality, but also suggest new ways for engineering the electronic structure of TMDs.

Isolation of a single sheet of graphene in 2004 [1] indicated that strictly two-dimensional (2D) materials can exist at finite temperatures. Indeed, inorganic 2D systems such as individual hexagonal BN and transition metal dichalcogenide (TMD) layers were later manufactured by mechanical [2,3] and chemical [4,5] exfoliation of their layered bulk counterparts, as well as by chemical vapor deposition [6,7]. Recently, TMDs with a common structural formula $MeX_2$, where Me stands for transition metals (Mo, W, Ti, etc.) and X for chalcogens (S, Se, Te), have received considerable attention. These 2D materials are expected to have electronic properties varying from metals to wide-gap semiconductors, similar to their bulk counterparts [8,9], and excellent mechanical characteristics [10]. The monolayer TMD materials have already shown a good potential in nanoelectronic [3,11,12] and photonic [4,13,14] applications.

Characterization of the *h*-BN [15–17] and TMD [5,6,18] samples has extensively been carried out using high-resolution transmission electron microscopy (HR-TEM). During imaging, however, energetic electrons in the TEM can give rise to production of defects due to ballistic displacements of atoms from the sample and beam-stimulated chemical etching [19], as studies on *h*-BN membranes also indicate [15–17,20].

Contrary to *h*-BN, very little is known about the effects of electron irradiation on TMDs. So far, atomic defects have been observed via HR-TEM in $WS_2$ nanoribbons encapsulated inside carbon nanotubes at electron acceleration voltage of 60 kV [21] as well as at the edges of $MoS_2$ clusters under 80 kV irradiation [22], while no significant

damage or amorphization was reported for $MoS_2$ sheets at 200 kV [18]—a surprising result taking into account the relatively low atomic mass of the S atom. Clearly, precise microscopic knowledge of defect production in TMDs under electron irradiation is highly desirable for assessing the effects of the beam on the samples. This knowledge would allow designing experimental conditions required to minimize damage, as well as developing beam-mediated postsynthesis doping techniques. Moreover, information on the displacement thresholds is important in the context of fundamental aspects of the interaction of beams of energetic particles with solids, as the reduced dimensionality may give rise to an irradiation response different from that in the bulk counterpart of the 2D material [23].

Here, by employing first-principles simulations, we study the behavior of a representative number of TMDs (21 compounds) under electron irradiation, and calculate the threshold energies for atomic displacements in each system, as well as displacement cross sections as functions of electron-beam energy. In the case of $MoS_2$, we also carry out HR-TEM experiments and provide evidence of electron-irradiation-induced production of vacancies in this material. In addition—inspired by the recent advances in introducing impurities in *h*-BN monolayers [24,25]—we discuss irradiation-mediated doping of TMD materials.

For all calculations in this work, we rely on the density-functional theory (DFT) with the Perdew-Burke-Ernzerhof (PBE) exchange-correlation functional [26] and the projector augmented wave formalism as implemented in the simulation package VASP [27,28]. In order to obtain a

comprehensive picture of the irradiation response of TMDs, we consider a large set of layered TMDs: $MoX_2$, $WX_2$, $NbX_2$, $TaX_2$, $PtX_2$, $TiX_2$, and $VX_2$ (where X = S, Se, or Te), which have similar crystal structures.

We started our study by calculating the displacement threshold energy $T_d$ (the minimum initial kinetic energy of the recoil atom) for sputtering an atom from the material. As in our previous simulations for graphene [29] and BN [20] monolayers, an initial velocity was assigned to the recoil atom (corresponding to instantaneous momentum transfer from the electron to the atom during the impact), then DFT molecular dynamics was used to model the time evolution of the system. In practice, the initial kinetic energy of the recoil atom was increased until it was high enough for the atom to be displaced from its lattice site without an immediate recombination with the resulting vacancy. The calculations were carried out using a $5 \times 5$ supercell of a $MeX_2$ monolayer. Test simulations for larger systems gave essentially the same results. The atomic structure of a $MoS_2$ layer and the simulation setup are shown in Fig. 1(a).

$T_d$ required for displacing a chalcogen atom from the bottom layer of the sheet [cf. Fig. 1(a)] is presented in Fig. 2. In addition to the prototypical $MoX_2$ and $WX_2$, we also present results for $TiS_2$ and $TiTe_2$. As evident from the figure, $T_d \in [5, 7]$ eV for all studied compounds.

We also calculated the vacancy formation energies ($E_f$) for each of the compounds to see how they correlate with $T_d$. We defined $E_f$ as

$$E_f = E_{\text{vac}} - (E_{\text{bulk}} - \mu_X), \qquad (1)$$

where $E_{\text{bulk}}$ and $E_{\text{vac}}$ are the energies of the pristine and vacancy containing supercells, respectively. The chemical potential $\mu_X$ of the chalcogen species is taken as the energy of the isolated atom to enable a straightforward comparison with the results of dynamical simulations. $E_f$, with and without relaxation of the atomic structure of the layer, is also presented in Fig. 2.
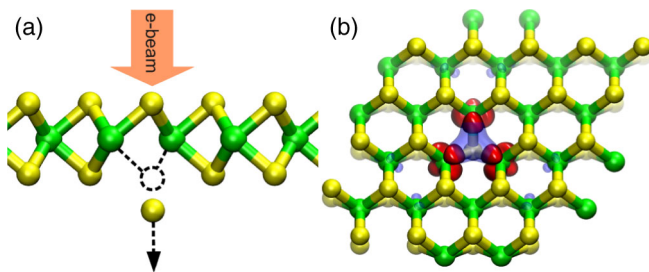


FIG. 1 (color online). (a) The setup used in the dynamical DFT simulations of atom sputtering from TMDs under electron irradiation. Initial energy acquired due to the impact of an energetic electron was assigned to the recoil atom, then DFT molecular dynamics was used to model the evolution of the system. (b) $MoS_2$ sheet with a S vacancy. The charge densities of the occupied and unoccupied defect states are visualized by transparent (blue) and solid (red) isosurfaces, respectively.

In the nonrelaxed case, the energetics is very similar for all materials, and—as can readily be noticed—the agreement between $T_d$ and the *nonrelaxed* $E_f$ is striking. This is because during the sputtering of chalcogen atoms from the outermost layer, little energy is transmitted to the surrounding metal atoms due to the sufficiently fast sputtering event and the rigidity of the structure. The energies for the relaxed geometries show a more intriguing behavior. Atomic relaxation for some systems evidently gives rise to a considerable drop in $E_f$, so that the similarity to $T_d$ is lost. This drop quantifies the degree of structural relaxation around the vacancy, which is minor for $MoS_2$; see Fig. 1(b). The analysis of the electronic structure revealed an occupied bonding type vacancy state close to valence band maximum and an empty antibonding type state in the mid gap, which stabilizes the structure. For the occupied bonding defect state, the electronic charge is localized at the vacancy site, analogous to bulk $MoS_2$, where Mo atoms donate electrons to S atoms. This is true for all of the semiconducting materials: $MoX_2$, $WX_2$, and $PtX_2$. The rest of the considered materials are metals or semimetals, for which the bonding vacancy state may become unoccupied, which is reflected in larger relaxation and lower formation energies.

Knowing $T_d$, it is possible to estimate the electron threshold energy through the relativistic binary collision formula and the atom displacement cross section (for relatively light atoms) by using the McKinley-Feshbach formalism [30]. $E_f$ for Se and Te compounds is smaller than in S compounds, but—due to the higher atomic mass—their creation through ballistic electron impacts requires significantly higher electron energies. In the case of $MoS_2$, $MoSe_2$, and $MoTe_2$, $T_d$ of 6.9, 6.4, and 5.9 eV correspond to electron energies of about 90, 190, and 270 keV, as calculated assuming a static lattice. For other compounds, the required electron energies
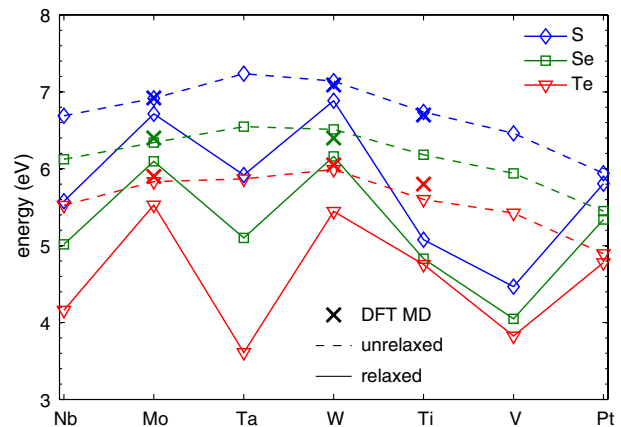


FIG. 2 (color online). Displacement threshold energies $T_d$ obtained from DFT molecular dynamics calculations (crosses) and formation energies of chalcogen vacancies with nonrelaxed (dashed lines) and relaxed (solid lines) geometries in transition metal dichalcogenides $MeX_2$, X = S, Se, Te.

should be of similar magnitude, based on the close values of $T_d$ in Fig. 2. An accurate estimation of the displacement cross section requires including the effects of lattice vibrations on the energy transferred from an electron to a target atom [31]. We calculated the cross sections for vacancy production as a function of electron energy for $MoS_2$, $WS_2$, and $TiS_2$ beyond the static lattice approximation, as shown in Fig. 3. We stress that the production of S vacancies for practically all TMDs is within the energies commonly used in TEM studies.

The displacement thresholds for chalcogen atoms in the (top) layer facing the beam proved to be considerably higher than for the bottom chalcogen layer, as the displaced atom is "stopped" by the other layers. However, after a vacancy is created in the bottom layer, the threshold energy for the top S atom in $MoS_2$ to be displaced and fill the vacancy is about 8.1 eV. This is similar in magnitude to the threshold for displacing S atom from the bottom layer (6.9 eV), and thus formation of vacancy columns should be possible even at 80 kV when lattice vibrations are accounted for. $T_d$ for transition metals is even higher, since they are bonded to six neighbors and similarly stopped by the S layer. For instance, about 20 eV is required to displace Mo atom from its site in the $MoS_2$ lattice, which corresponds to electron energy of 560 keV. Naturally, under such conditions the S sublattice is quickly destroyed. Formation of transition metal vacancies is thus considered highly unlikely.

With regard to possible vacancy agglomeration under continuous irradiation, we found that creation of a vacancy does not alter the formation energy in the neighboring sites in the semiconducting TMDs. Thus, we do not expect accelerated formation of large vacancy clusters. In the
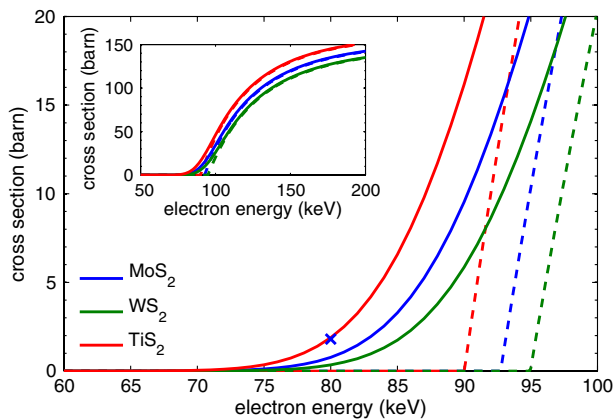


FIG. 3 (color online).  Cross section for sputtering a sulfur atom from $MoS_2$, $WS_2$, and $TiS_2$ sheets as calculated through the McKinley-Feshbach formalism and the dynamical values of the displacement thresholds. Dotted lines are the data for the static lattice, and solids lines are the results of calculations where lattice vibrations are taken into account, assuming a Maxwell-Boltzmann velocity distribution. The cross denotes the experimentally determined cross section for $MoS_2$. The inset shows the same data for a larger range of electron energies.

same vein, however, it is worth noting that chalcogen atoms may also be sputtered fairly easily from the edges of nanostructures [21,22]. For example, our calculations for a $WS_2$ ribbon show that the chalcogen atoms at the edge can have a displacement threshold as low as 4.2 eV, as compared to 7.0 eV away from the edge.

To check our theoretical results on irradiation-induced vacancy formation in $MoS_2$, we experimentally studied the evolution of a $MoS_2$ sheet under an 80 keV electron beam. First, freestanding single-layer $MoS_2$ samples were prepared by mechanical exfoliation of natural $MoS_2$ bulk crystals, followed by characterization via optical microscopy on a $Si + 90$ nm $SiO_2$ substrate and transfer to a perforated TEM support film (Quantifoil), similar to graphene samples [32]. The TEM grid was adhered to the $SiO_2$ surface by evaporating isopropanol on top of it. After this, the silica was etched with KOH. Aberration-corrected (AC) HR-TEM imaging was carried out in an image-side Cs-corrected FEI TITAN microscope at a primary beam energy of 80 keV. The contrast difference between the Mo and S sublattice is clearly detectable in the AC HR-TEM images proving the single-layer nature of the sheet (for a double layer, the contrast would be identical as Mo is stacked above S). This is also confirmed in diffraction measurements, as successive diffraction spots from one $\{hkl\}$ family show different intensity, whereas for bi- and multilayers they are equal [18]. The analyzed intensity ratio of the $\{\bar{1}100\}$ diffraction spots was found to be 1.07.

During continuous imaging we found an increasing number of vacancy sites (exclusively on the S sublattice) accompanied by crack formation [see Fig. 4(a)] and lateral shrinkage of the membrane. Counting the actual number of sputtered atoms as in Ref. [31], the cross section for sputtering was found to be 1.8 b, which is in a reasonable agreement with the calculated cross section of 0.8 b, taking into account that the theoretical estimates are very sensitive to inaccuracies in the parameters of the model (e.g., $T_d$ and the velocity distribution) at energies below the static threshold.

In Figs. 4(d) and 4(e) we present simulated TEM images [33] for the single and double vacancies, respectively, based on atomic structures [Figs. 4(b) and 4(c)] obtained from the DFT calculations. Similar defects are observed in the experimental TEM images [Fig. 4(f)]. Different defects can clearly be distinguished by analyzing the (Michelson) contrast relative to the contrast of the Mo atoms in the pristine area. We find that the experimental (simulated) ratios are 0.9 (0.9) for a sulfur column, 0.5 (0.4) for the single and 0.2 (0.2) for the double vacancy.

Having shown that vacancies can be created in TMDs under electron irradiation, we move on to study whether they could be consecutively filled with other atomic species deliberately introduced into the TEM chamber. We calculate the formation energy of substitutional defects in $MoS_2$ and consider donors F, Cl, Br, and I; acceptors, N, P, As, and Sb; double acceptors C and Si; hydrogen H and $H_2$;
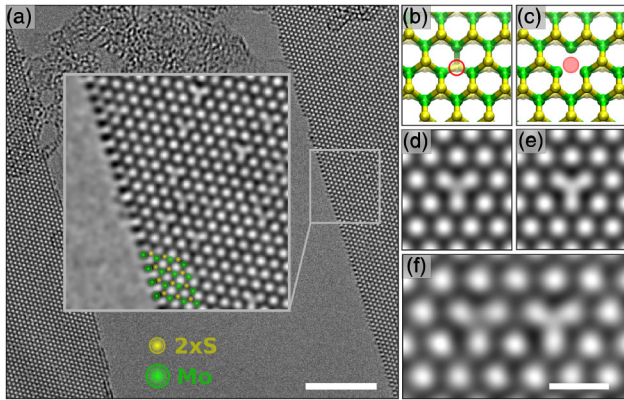
FIG. 4 (color online). AC HR-TEM images of single-layer $MoS_2$. Atoms are dark and white spots correspond to the holes in the hexagonal structure. During continuous 80 keV electron irradiation, a crack formed in the membrane (a). The edges are terminated with Mo atoms, as can be determined from the contrast in the inset. Also an increasing number of S vacancies is observed. Most of them are single vacancies but also double vacancies, where the top and bottom S atoms are removed, can be found. Structure models and corresponding HR-TEM image simulations for both vacancy types are shown in (b),(d) for the single and (c),(e) for the double vacancy. Experimental examples are shown in (f). To enhance the visibility of the defect, a Gaussian filter (0.7 Å FWHM) was applied to (d), (e), and (f). Scale bars are 5 nm (a) and 5 Å (f).



FIG. 5 (color online). (a) Substitution energies of the impurity atoms in $MoS_2$ layer calculated for three different chemical potentials: isolated atoms (plus, blue), diatomic molecules (dot, red), and molecules with hydrogen (cross, green). The solid phase reference is also given for carbon and silicon (black). (b) Respective local density of states of the impurity atoms, the spin-up and spin-down components. The gray areas denote the band edges of the $MoS_2$ layer. (c)–(e) Series of AC HR-TEM images demonstrating vacancy filling. The left arrow (red) highlights an initial S vacancy that picks up an atom between (d) and (e), and the right arrow (green) indicates a S atom that is sputtered away between (c) and (d), forming a single vacancy.

and isoelectronic species O, S, Se, and Te. The formation energies and the local density of states (LDOS) around the substitution site are shown in Fig. 5. We list the formation energies with three different chemical potentials of the substituted (impurity) species: the isolated atoms, diatomic molecules, or molecules with hydrogen ($CH_4$, $SiH_4$, $NH_3$, $PH_3$, $AsH_3$, HF, HCl, and HBr), where we set $\mu_H = \frac{1}{2} E_{H_2}$.

Because of the high formation energy of the vacancy, all substitutions are energetically favored with respect to the isolated atom. However, with respect to $\mu$ in the molecule, C, Si, and N substitutions have positive formation energies. Obviously, even if the equilibrium energetics does not favor the formation of the substitutional defect, the substitution may still be achieved under an electron beam, because molecules like $N_2$ or hydrocarbons will constantly break apart under the electron beam, and possibly due to electrical charging of the sample [34]. Thus postsynthesis electron-mediated doping may also be realized in 2D TMDs, similar to BN sheets [24,25]. The LDOS shows that N, P, As, and Sb behave as acceptors, whereas F, Cl, Br, and I are likely to be donors. C and Si have levels in the middle of the gap and the isoelectronic species like O, Se, or Te do not produce any localized states, as expected.

Filling of the vacancies was also observed in the TEM images, as shown in the series of panels in Figs. 5(c)–5(e). Although we could not identify the type of the impurity, this example proves that electron-beam-mediated doping is possible. Consequently, through control of atomic species
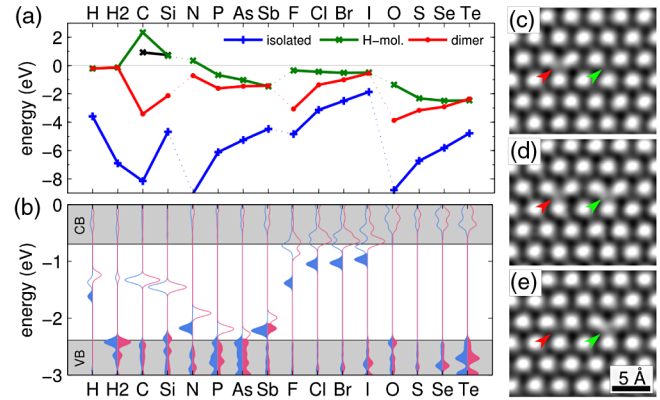
in the TEM chamber and the choice of the electron energy, modification of the physical properties of TMDs via electron beam should be attainable.

To conclude, we calculated atom displacement threshold energies in a number of TMDs. These energies are a measure of the radiation hardness of the material, and serve as critical input parameters in the Kinchin-Pease and other semiclassical theories of defect production and ion stopping [23,35]. Here we use them to calculate electron displacement energies and corresponding sputtering cross sections to quantitatively assess the amount of damage created in 2D TMD materials during a TEM experiment via knock-on processes. Observations of vacancies in our experimental AC HR-TEM images of single $MoS_2$ sheets validate our theoretical predictions. Finally, we observe filling of the vacancies and discuss the prospects for electron-beam mediated doping of TMDs.

[1] K. S. Novoselov, A. K. Geim, S. V. Morozov, D. Jiang, Y. Zhang, S. V. Dubonos, I. V. Grigorieva, and A. A. Firsov, Science **306**, 666 (2004).

[2] K. S. Novoselov, D. Jiang, F. Schedin, T. J. Booth, V. Khotkevich, S. Morozov, and A. K. Geim, Proc. Natl. Acad. Sci. U.S.A. **102**, 10451 (2005).

[3] B. Radisavljevic, A. Radenovic, J. Brivio, V. Giacometti, and A. Kis, Nature Nanotech. **6**, 147 (2011).

[4] G. Eda, H. Yamaguchi, D. Voiry, T. Fujita, and M. Chen, Nano Lett. **11**, 5111 (2011).

[5] J. N. Coleman, M. Lotya, A. O'Neill, S. D. Bergin, P. J. King, U. Khan, K. Young, A. Gaucher, S. De, R. J. Smith, I. V. Shvets, S. K. Arora, G. Stanton, H.-Y. Kim, K. Lee, G. T. Kim, G. S. Duesberg, T. Hallam, J. J. Boland, J. J. Wang, J. F. Donegan, J. C. Grunlan, G. Moriarty, A. Shmeliov, R. J. Nicholls, J. M. Perkins, E. M. Grieveson, K. Theuwissen, D. W. McComb, P. D. Nellist, and V. Nicolosi, Science **331**, 568 (2011).

[6] K. Kim, A. Hsu, X. Jia, S. Kim, Y. Shi, M. Hofmann, D. Nezich, J. Rodriguez-Nieva, M. Dresselhaus, T. Palacios, and J. Kong, Nano Lett. **12**, 161 (2012).

[7] Y. Zhan, Z. Liu, S. Najmaei, P. M. Ajayan, and J. Lou, Small **8**, 966 (2012).

[8] J. Wilson and A. Yoffe, Adv. Phys. **18**, 193 (1969).

[9] C. Ataca, H. Şahin, and S. Ciraci, J. Phys. Chem. C **116**, 8983 (2012).

[10] A. Castellanos-Gomez, M. Poot, G. a Steele, H. S. J. van der Zant, N. Agraït, and G. Rubio-Bollinger, Adv. Mater. **24**, 772 (2012).

[11] H. Li, Z. Yin, Q. He, H. Li, X. Huang, G. Lu, D. W. H. Fam, A. I. Y. Tok, Q. Zhang, and H. Zhang, Small **8**, 63 (2012).

[12] I. Popov, G. Seifert, and D. Tománek, Phys. Rev. Lett. **108**, 156802 (2012).

[13] K. F. Mak, C. Lee, J. Hone, J. Shan, and T. F. Heinz, Phys. Rev. Lett. **105**, 136805 (2010).

[14] Z. Yin, H. Li, H. Li, L. Jiang, Y. Shi, Y. Sun, G. Lu, Q. Zhang, X. Chen, and H. Zhang, ACS Nano **6**, 74 (2012).

[15] J. C. Meyer, A. Chuvilin, G. Algara-Siller, J. Biskupek, and U. Kaiser, Nano Lett. **9**, 2683 (2009).

[16] C. Jin, F. Lin, K. Suenaga, and S. Iijima, Phys. Rev. Lett. **102**, 195505 (2009).

[17] J. C. Meyer, S. Kurasch, H. J. Park, V. Skalakova, D. Kunzel, A. Gross, A. Chuvilin, G. Algara-Siller, S. Roth, T. Iwasaki, U. Starke, J. H. Smet, and U. Kaiser, Nature Mater. **10**, 209 (2011).

[18] J. Brivio, D. T. L. Alexander, and A. Kis, Nano Lett. **11**, 5148 (2011).

[19] K. Mølhave, S. B. Gudnason, A. T. Pedersen, C. H. Clausen, A. Horsewell, and P. Bggild, Ultramicroscopy **108**, 52 (2007).

[20] J. Kotakoski, C. H. Jin, O. Lehtinen, K. Suenaga, and A. V. Krasheninnikov, Phys. Rev. B **82**, 113404 (2010).

[21] Z. Liu, K. Suenaga, Z. Wang, Z. Shi, E. Okunishi, and S. Iijima, Nature Commun. **2**, 213 (2011).

[22] L. P. Hansen, Q. M. Ramasse, C. Kisielowski, M. Brorson, E. Johnson, H. Topsøe, and S. Helveg, Angew. Chem., Int. Ed. **50**, 10153 (2011).

[23] A. V. Krasheninnikov and K. Nordlund, J. Appl. Phys. **107**, 071301 (2010).

[24] X. Wei, M. Wang, Y. Bando, and D. Golberg, ACS Nano **5**, 2916 (2011).

[25] O. L. Krivanek, M. F. Chisholm, V. Nicolosi, T. J. Pennycook, G. J. Corbin, N. Dellby, M. F. Murtt, C. S. Own, Z. S. Szilagyi, M. P. Oxley, S. T. Pantelides, and S. J. Pennycook, Nature (London) **464**, 571 (2010).

[26] J. P. Perdew, K. Burke, and M. Ernzerhof, Phys. Rev. Lett. **77**, 3865 (1996).

[27] G. Kresse and J. Hafner, Phys. Rev. B **47**, 558 (1993).

[28] G. Kresse and J. Furthmuller, Comput. Mater. Sci. **6**, 15 (1996).

[29] J. Kotakoski, D. Santos-Cottin, and A. V. Krasheninnikov, ACS Nano **6**, 671 (2012).

[30] W. A. McKinley and H. Feshbach, Phys. Rev. **74**, 1759 (1948).

[31] J. C. Meyer, F. Eder, S. Kurasch, V. Skakalova, J. Kotakoski, H. J. Park, S. Roth, A. Chuvilin, S. Eyhusen, G. Benner, A. V. Krasheninnikov, and U. Kaiser, Phys. Rev. Lett. **108**, 196102 (2012).

[32] J. C. Meyer, C. O. Girit, M. F. Crommie, and a. Zettl, Appl. Phys. Lett. **92**, 123110 (2008).

[33] C. Koch, Ph.D. thesis, Arizona State University, 2002.

[34] N. Berseneva, A. V. Krasheninnikov, and R. M. Nieminen, Phys. Rev. Lett. **107**, 035501 (2011); **107**, 239602 (2011).

[35] G. H. Kinchin and R. S. Pease, Rep. Prog. Phys. **18**, 1 (1955).